

Scour Effect on Dynamic Characteristics and Responses of Offshore Wind Turbines

Dongyue Tang¹ and Ming Zhao^{1, *}

Abstract: The monopile foundation is the main form of offshore wind turbine foundation, and its surrounding scouring pit will reduce the constraints of the soil on the piles, which makes wind turbine foundation instability a key issue affecting the structural safety of offshore wind turbines. In previous studies, the rotating rotor and control system are neglected when studying the influence of scour on the offshore wind turbine structure. In this paper, the numerical model of the blade-tower-monopile integrated offshore wind turbine is established, and the influence of scour on the dynamic characteristics of wind turbine is obtained considering parameters, such as blade azimuth, pitch angle, rotor speed, and soil stiffness. After calculating wind load by using the modified Blade Element Momentum theory, the impact of scour on the wind-induced response of a monopile wind turbine is achieved, considering control system and aeroelastic coupling. Therefore, a reference method is proposed for estimating scour depth according to the monopile foundation offshore wind turbine wind-induced response.

Keywords: Scour effect, offshore wind turbine, dynamic characteristics, dynamic response.

1 Introduction

At present, the monopile foundation is the main form of foundation for offshore wind turbines, accounting for 80% of foundations for engineering applications [Ho, Mbistrova and Corbetta (2016)]. The presence of piles impedes the flow of water, causing the flow of water to form vortices around the piles, which take away the soil around the piles, creating a scour hole around each of them [Pournazeri, Li and Haghghat (2015)]. Most scholars believe that there is a maximum scour depth, and it is related to the pile diameter [Sumer, Fredsøe and Christiansen (1992); Veritas (2010)]. For example, Zaaier and Van der Tempel [Zaaier and Van der Tempel (2004)] considers the scour depth to be $0.8-2.5D$, where D is the pile diameter. As the diameter of the monopile foundation of

¹ College of Civil Engineering, Tongji University, Shanghai, China.

* Corresponding Author: Zhao Ming. Email: zhaom@tongji.edu.cn.

Received: 28 November 2019; Accepted: 21 April 2020.

the offshore wind turbine increases, the scour depth will increase, and the influence of the scour depth of the monopile foundation wind turbine will also increase.

Because a monopile foundation is mainly used to transmit lateral force, and most of the force is transmitted through the upper layer soil, a tubular tower on a monopile foundation is more affected by scour than a tripod foundation and a lattice tower with piles [Van der Tempel, Zaaier and Subroto (2004); Zaaier and Van der Tempel (2004)].

Scholars have mainly analyzed the impact of scouring on a wind turbine from the perspective of frequency, because the wind turbine design frequency is between the rotor rotational frequency ($1P$) and the blade passage frequency (for the three-blade wind turbine, $3P$). Scouring causes the wind turbine frequency to decrease, creating a resonance risk [Prendergast, Gavin and Doherty (2015); Prendergast, Reale and Gavin (2018)]. Sørensen and Ibsen [Sørensen and Ibsen (2013)] performed a numerical simulation of a 2-MW wind turbine to analyze the effect of the scour depth on the frequency. It was found that the frequency was reduced by 5% when the scour depth was $1.3D$. Abhinav and Saha [Abhinav and Saha (2016)] found that due to the rigid body rotation of the monopile foundation under the condition of loose sand, the structural frequency and the horizontal response of the pile top increased with decreasing sand density under the same depth. However, the above literature simplifies the rotor to a concentrated mass when using numerical simulation to calculate the influence of the scouring on wind turbine. This method ignores the interaction between the rotor and tower, this is because wind turbine blade is so complicate that scholars have modeled it separately without a tower [Lin, Lee and Lin (2008); Yang, Peng, Cao et al. (2014)]. However, the wind turbine is an integrated structure including a rotor, nacelle, tower, and foundation, and the rotating rotor at the top of the tower is an important feature of the wind turbine. Therefore, the calculation result based on simplifying the rotor to a concentrated mass is inaccurate.

In designing a wind turbine control system, scholars have established different numerical calculation models for wind turbines considering the coupling of the rotor and tower [Staino and Basu (2013); Zhang (2015); Zhang, Li, Nielsen et al. (2014); Zhang, Nielsen, Blaabjerg et al. (2014)]. This kind of numerical model can consider the gravity effect and centrifugal stiffening of the blade rotation, but a fixed foundation is mainly used as the wind turbine foundation. In fact, offshore wind turbines are more complex than onshore wind turbines because of pile-soil interactions [Zaaier (2006)]. Fitzgerald and Basu [Fitzgerald and Basu (2016)] used a bi-axial rotational spring to simulate a gravity-based wind turbine, and compared the calculation results with a fully fixed wind turbine model, and obtained the conclusion that pile-soil interaction will affect the structure frequency. However, this method of foundation simplification is not suitable for monopile foundation wind turbines, because the bi-axial rotational spring cannot effectively simulate the pile-soil interaction around monopile foundation.

The current research on monopile foundation wind turbines is mainly carried out in two aspects. one of which to simplify the rotor to mass for tower and foundation dynamic analysis, and the other is to simplify the wind turbine foundation to fixed end for rotor

dynamic analysis. The above research aspects are combined in this paper, a dynamic numerical model of a rotor-tower-foundation integrated monopile foundation wind turbine is proposed. Based on the numerical model, the influence of scouring on the dynamic characteristics of a monopile foundation wind turbine can be calculated considering several parameters, e.g., blade azimuth, pitch angle, rotor speed, and soil parameters. Furthermore, in this paper the corrected Blade Element Momentum theory is used to calculate the wind load and the influence of scouring on the wind-induced response of a monopile-foundation variable-speed variable-pitch offshore wind turbine, considering the control system and aeroelastic coupling.

2 Offshore wind turbine model

2.1 Offshore wind turbine model

Two types of coordinate systems are adopted in the proposed model—the global and blade local coordinate systems—and the schematic representation of the coordinate systems is shown in Fig. 1. The origin of the global coordinate system, represented by O , is the intersection of the pile without deformation and the mudline of the foundation without scouring. There is a blade local coordinate system for each blade. The blade number is

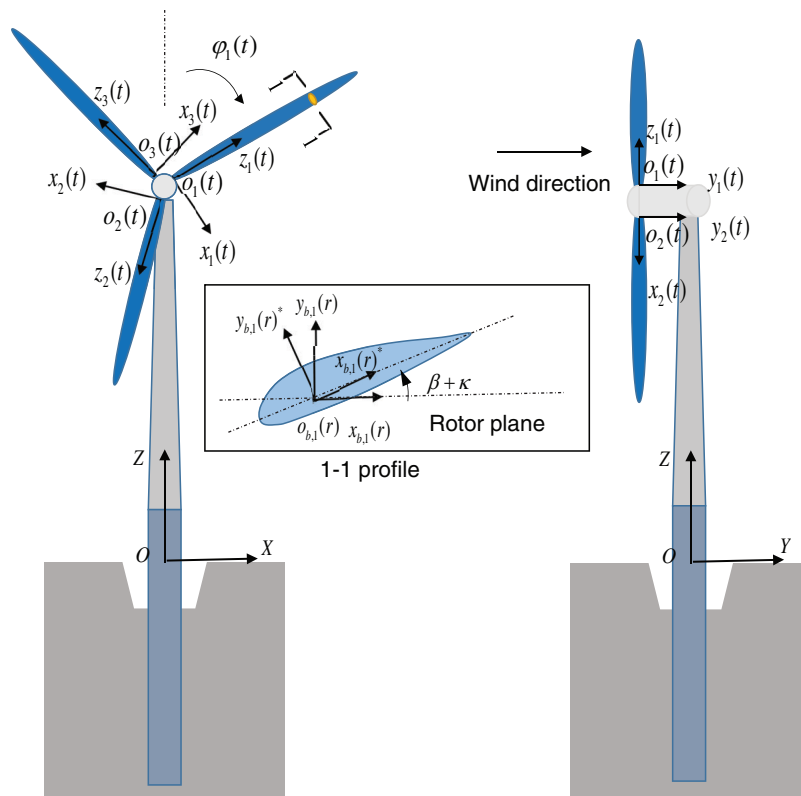


Figure 1: Coordinate systems of offshore wind turbine

denoted by i ($i=1, 2, 3$), while three blades are marked in the clockwise direction. The blade azimuth angle at time t is represented by $\varphi_i(t)$. The origin of the blade local coordinate system, represented by $o_i(t)$, is the root of blade i , and the axis $z_i(t)$ is along the spanning direction of blade i . Both coordinate axis and the origin change with time.

The axis $x_i(t)$ is in the rotor plane, and the axis $y_i(t)$ is perpendicular to the rotor plane. As for each blade profile, the angle between the blade profile main axis and rotor plane is the sum of the pre-twist angle κ and the pitch angle β .

The offshore wind turbine model has a total of eight generalized degrees of freedom, as shown in Fig. 2. The first two generalized degrees of freedom, represented by $q_{t,x}(t)$ and $q_{t,y}(t)$, are bi-axial displacements at the top of the tower. Other generalized degrees of freedom are related to the three blades. Regarding blade i , there are two generalized degrees of freedom, denoted $q_{xb,i}(t)$ and $q_{yb,i}(t)$, representing displacement at the blade tip along the x_i and y_i axis, respectively, of the blade.

After the coordinate system and degrees of freedom are clarified, the Lagrange equation is used to obtain the equation of motion for the offshore wind turbine:

$$\frac{d}{dt} \left(\frac{\partial T}{\partial \dot{q}_j} \right) - \frac{\partial T}{\partial q_j} + \frac{\partial V}{\partial q_j} = Q \quad (1)$$

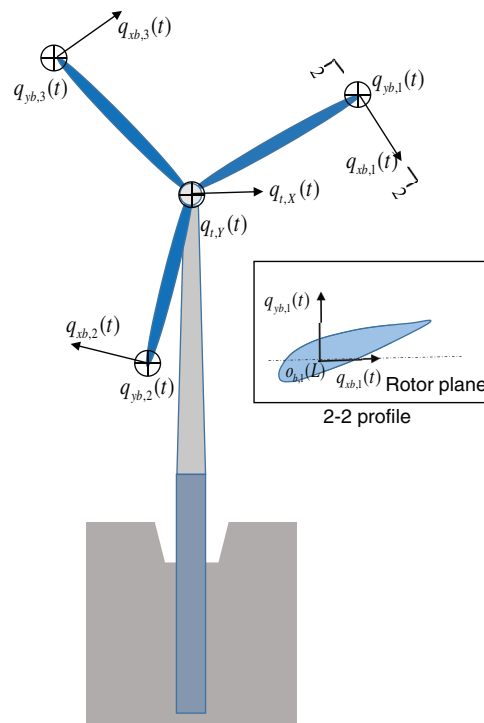


Figure 2: Degrees of freedom for offshore wind turbine model

where T signifies the total kinetic energy, V is the total potential energy, Q is the generalized force, and q_j is the j th generalized degree of freedom given in Fig. 2.

The expression of the total kinetic energy T is:

$$T = \frac{1}{2} \sum_{i=1}^3 \int_0^L \mu(r) v_i^2 dr + \frac{1}{2} \int_{-d-S}^H \mu_t(h) v_t^2(h) dh + \frac{1}{2} M_{hn} (\dot{q}_{t,X}^2 + \dot{q}_{t,Y}^2) \quad (2)$$

where M_{hn} represents the total mass of the hub and nacelle, and H , d , and S represent the height of the support structure above the mudline, pile penetration length, and scour depth, respectively, as shown in Fig. 3. $\dot{q}_{t,X}$ and $\dot{q}_{t,Y}$, which are also the first derivatives of the degree of freedom for the support structure, represent the velocities at top of the tower. $v_t(h) = [\dot{u}_{t,X}(h, t), \dot{u}_{t,Y}(h, t)]$ is the velocity vector of the support structure, which includes the tower and monopile, at height h . $\mu(r)$ and $\mu_t(h)$ are variable masses per unit length of the blade and support structure, respectively. Ω represents the rotational speed of the rotor. The term v_i is the absolute speed of the blade section, which cannot be directly derived from the first derivative of the degree of freedom for the blade, and v_i is expressed as follows:

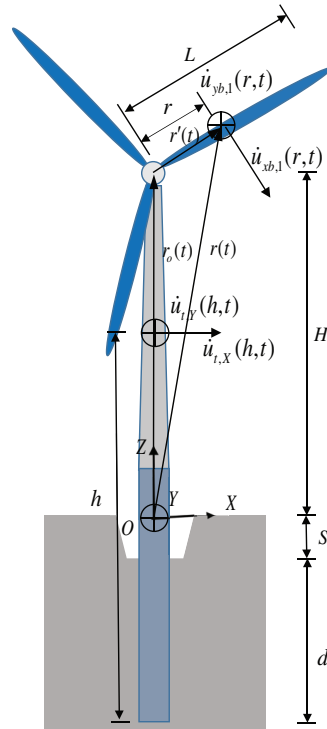


Figure 3: Velocity for arbitrary position for blade, tower, and monopile

$$\begin{aligned}
v_i &= \dot{r}_o(t) + w(t) \times r'(t) + v'(t) \\
&= \begin{bmatrix} \dot{q}_{t,X} \cos \varphi_i \\ \dot{q}_{t,Y} \\ \dot{q}_{t,X} \sin \varphi_i \end{bmatrix} + \begin{bmatrix} 0 \\ \Omega(t) \\ 0 \end{bmatrix} \times \begin{bmatrix} u_{xb,i} \\ u_{yb,i} \\ r \end{bmatrix} + \begin{bmatrix} \dot{u}_{xb,i} \\ \dot{u}_{yb,i} \\ 0 \end{bmatrix} = \begin{bmatrix} \dot{q}_{t,X} \cos \varphi_i + \dot{u}_{xb,i} + \Omega r \\ \dot{q}_{t,Y} + \dot{u}_{yb,i} \\ \dot{q}_{t,X} \sin \varphi_i - \Omega u_{xb,i} \end{bmatrix} \quad (3)
\end{aligned}$$

where $\dot{r}_o(t)$ represents the absolute velocity vector at the top of the tower in the global coordinate system, as shown in Fig. 3. $r'(t)$ and $v'(t)$ are respectively the relative displacement and velocity vectors of a blade i section relative to the top of the tower under the local coordinate of the blade i . $w(t)$ represents the rotational angular velocity vector.

The total potential energy V is expressed as:

$$\begin{aligned}
V &= \frac{1}{2} \sum_{i=1}^3 (k_{e,y} + k_{g,y} + k_{gr,y}) q_{xb,i}^2 + \frac{1}{2} \sum_{i=1}^3 (k_{e,x} + k_{g,x} + k_{gr,x}) q_{yb,i}^2 + \sum_{i=1}^3 k_c q_{xb,i} q_{yb,i} \\
&\quad + \frac{1}{2} (k_{t,Y} + k_{s,X} + k_{gr,X}) q_{t,X}^2 + \frac{1}{2} (k_{t,X} + k_{s,Y} + k_{gr,Y}) q_{t,Y}^2 \quad (4)
\end{aligned}$$

where $k_{e,x}$ and $k_{e,y}$ represent the bi-axial elastic stiffnesses of the blade, which are expressed as:

$$k_{e,x} = \int_0^L EI_x(r) (\phi_y''(r))^2 dr \quad (5)$$

$$k_{e,y} = \int_0^L EI_y(r) (\phi_x''(r))^2 dr \quad (6)$$

in which, and $I_x(r)$ and $I_y(r)$ are moment of inertia about $x_{b,i}(r)$ and $y_{b,i}(r)$ respectively, which are shown in Fig. 1, and they can be obtained by:

$$I_x(r) = \frac{I_x(r)^* + I_y(r)^*}{2} - \frac{I_x(r)^* - I_y(r)^*}{2} \cos(-2(\kappa + \beta)) \quad (7)$$

$$I_y(r) = \frac{I_x(r)^* + I_y(r)^*}{2} + \frac{I_x(r)^* - I_y(r)^*}{2} \cos(-2(\kappa + \beta)) \quad (8)$$

where $I_x(r)^*$ and $I_y(r)^*$ are moment of inertia about $x_{b,i}(r)^*$ and $y_{b,i}(r)^*$ respectively, which are shown in Fig. 1. In Eqs. (5)-(6), ϕ_x and ϕ_y are bi-axial mode shapes for blade. $k_{g,x}$ and $k_{g,y}$ in Eq. (4) are the bi-axial centrifugal stiffnesses of the blade due to blade rotation, and $k_{gr,x}$ and $k_{gr,y}$ indicate centripetal or centrifugal stiffnesses, resulting from the force of blade gravity projection on the $z_i(t)$ axis. The term k_c represents the bi-axial coupling stiffness of the blade due to the pre-twist angle and pitch angle; see the reference [Fitzgerald and Basu (2016)] for the blade stiffnesses expressions. Regarding the support structure, vibration modes of the support structure should be defined first, and ϕ_X and ϕ_Y are used to signify vibration modes with respect to the X and Y -axis, respectively. The terms $EI_{t,x}$ and $EI_{t,y}$

indicate the respective bi-axial stiffnesses of the support structure. The terms $k_{t,X}$ and $k_{t,Y}$ in Eq. (4) indicate the respective bi-axial elastic stiffnesses after scouring, changing with scour depth, which can be expressed as follows:

$$k_{t,Y}(S) = \int_{-d-S}^H EI_{t,Y}(h) (\phi_X''(h, S))^2 dh \quad (9)$$

$$k_{t,X}(S) = \int_{-d-S}^H EI_{t,X}(h) (\phi_Y''(h, S))^2 dh \quad (10)$$

$k_{gr,X}$ and $k_{gr,Y}$ in Eq. (4) denote the geometric stiffnesses of the support structure separately relative to the X and Y axes after scouring, respectively, resulting from the gravity of the total top mass and support structure itself, which are expressed as follows:

$$k_{gr,Y}(S) = -g \int_{-d-S}^H \left(\int_h^H \mu_t(\xi) \xi d\xi \right) (\phi_Y'(h, S))^2 dh - m_{top} g \int_{-d-S}^H (\phi_Y'(h, S))^2 dh \quad (11)$$

$$k_{gr,X}(S) = -g \int_{-d-S}^H \left(\int_h^H \mu_t(\xi) \xi d\xi \right) (\phi_X'(h, S))^2 dh - m_{top} g \int_{-d-S}^H (\phi_X'(h, S))^2 dh \quad (12)$$

where m_{top} signifies the total mass of blades, hub, and nacelle. $k_{S,X}$ and $k_{S,Y}$ are the respective bi-axial stiffnesses by pile-soil interaction after scouring. As a distributed spring is used in this paper for foundation modeling, per-unit-height pile-soil-interaction stiffness is expressed by per-unit-height stiffness of the distributed spring, represented by k_{soil} . As shown in Fig. 4, layered soil is taken as an example, the height of distributed springs decreased after scouring and the reduction is same as the scour depth. The formulas for $k_{S,X}$ and $k_{S,Y}$ are:

$$k_{S,X}(S) = \int_{-d}^{-S} k_{soil}(h, S) (\phi_X''(h, S))^2 dh \quad (13)$$

$$k_{S,Y}(S) = \int_{-d}^{-S} k_{soil}(h, S) (\phi_Y''(h, S))^2 dh \quad (14)$$

By substituting Eqs. (5)-(14) into Eq. (4), the total potential energy V can be obtained. Furthermore, the equation of motion for an offshore wind turbine under free vibration conditions, in the form of Eq. (15), can be obtained by substituting Eqs. (2) and (3) into Eq. (1):

$$M\ddot{q} + C\dot{q} + Kq = 0 \quad (15)$$

where M , K , and C indicate the mass matrix, stiffness matrix, and damping matrix of the offshore wind tower, respectively, and are defined in Appendix A.

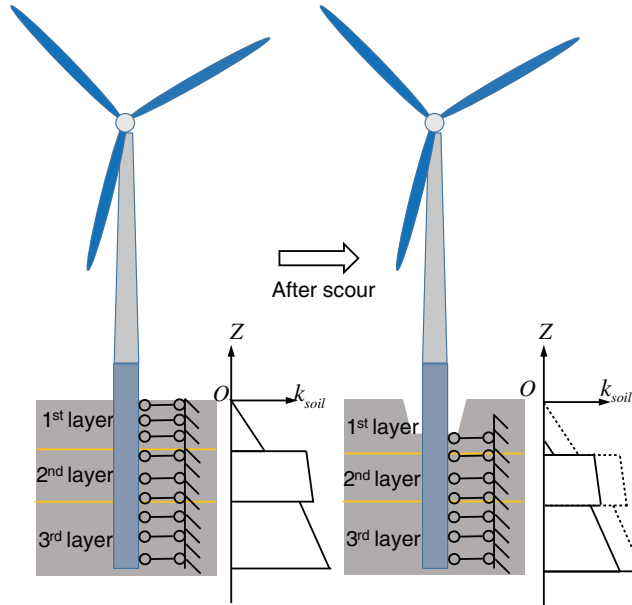


Figure 4: Schematic of stiffness change due to scour depth

2.2 Wind turbine loading

2.2.1 Aerodynamic loading

The law of average wind speed as a function of height can be described by an exponential function [Davenport (1965)], i.e.,

$$\frac{\bar{V}(z)}{\bar{V}(z_h)} = \left(\frac{z}{z_h}\right)^{\alpha_2} \quad (16)$$

where α_2 is the ground roughness coefficient and $\bar{V}(z)$ the average wind speed at height z , with z_h being the standard reference height. The wind speed time history point of a rotating blade is called the rotary sampled wind speed. Since the wind speed profile is considered, peaks appear at a multiple of the rotational frequency of the rotor for the power spectral density curve of the uniformly rotating blade.

The aerodynamic load of the blade is calculated by the modified Blade Element Momentum (BEM) theory. A micro-segment, which at a distance from the blade root is taken as r , is shown in Fig. 5(a), the profile of which is displayed in Fig. 5(b). The wind speed depicted by the segment in Fig. 5(b) is called the relative wind speed, denoted by V_{rel} , and it can be decomposed into a component V_y perpendicular to the rotor plane and a component V_x parallel to the rotor plane. The out-of-plane velocity V_y and in-plane velocity V_x can be expressed as:

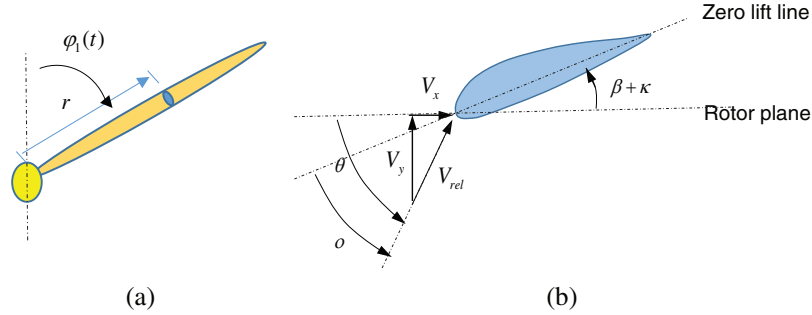


Figure 5: Schematic of Blade Element Momentum theory

$$\begin{aligned} V_y &= \bar{V}(z)(1-a) \\ V_x &= \Omega r(1+a') \end{aligned} \quad (17)$$

$$V_{rel} = \sqrt{V_x^2 + V_y^2} = \sqrt{(1-a)^2 \bar{V}(z)^2 + (1+a')^2 (\Omega r)^2} \quad (18)$$

where a and a' represent the axial and the circumferential induced velocity, respectively, and Ω is the rotating speed of the rotor.

In Fig. 5(b), θ is the angle between the rotor plane and the relative velocity V_{rel} , and the expression of the in-flow angle θ at the blade segment is:

$$\theta = \arctan\left(\frac{V_x}{V_y}\right) \quad (19)$$

The expression of the local angle of attack o is:

$$o = \theta - \beta - \kappa \quad (20)$$

The lift coefficient C_L and drag coefficient C_D can be determined based on the local angle of attack o , so that the normal coefficient C_N and tangential coefficient C_T can be derived by coordinate transformation according to Fig. 6. The normal force dp_N and the tangential force dp_T on one segment resulting from wind velocity V_{rel} can be calculated as follows:

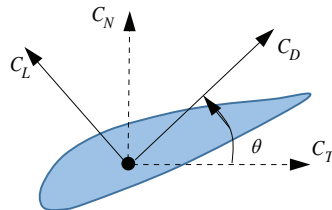


Figure 6: Schematic of coordinate transformation of lift and drag coefficients

$$dp_N = \frac{1}{2} \rho V_{rel}^2(r, t) c(r) C_N(o) dr \quad (21)$$

$$dp_T = \frac{1}{2} \rho V_{rel}^2(r, t) c(r) C_T(o) dr \quad (22)$$

where c is the section chord length. The expressions for generalized aerodynamic loading of all the degrees of freedom are

$$\begin{aligned} Q_{xb,i} &= \int_0^L p_{T,i}(r, t) \phi_x(r) dr \\ Q_{yb,i} &= \int_0^L p_{N,i}(r, t) \phi_y(r) dr \\ Q_{t,Y} &= \sum_{i=0}^3 P_{yb,i}(t) \\ Q_{t,X} &= \sum_{i=0}^3 p_{T,i}(r, t) \cos \varphi_i \end{aligned} \quad (23)$$

where $Q_{xb,i}$ is the generalized aerodynamic loading along the x_i axis at the tip of blade i , corresponding with degree of freedom $q_{xb,i}$, and $Q_{yb,i}$ is the generalized aerodynamic loading along the y_i axis at the tip of blade i , corresponding to degree of freedom $q_{yb,i}$. Similarly, $Q_{t,X}$ and $Q_{t,Y}$ are the bi-axial generalized aerodynamic loadings at the tower top in the global coordinate system, related to $q_{t,X}$ and $q_{t,Y}$ respectively.

2.2.2 Gravity loading

The blade gravity can be decomposed into two separate component forces along the z_i and x_i axes. The former has been accounted for as centrifugal or centripetal force when calculating blade stiffness, and the latter has an influence on the displacement $q_{xb,i}(t)$, which is also called the blade-tip in-plane displacement. The generalized gravity loading for the support structure is 0, and the general gravity loading for degrees of freedom $q_{xb,i}$ is denoted $Q_{i,g}$, which is expressed as follows:

$$Q_{i,g} = \int_0^L \mu(r) \phi_x(r) g \sin \varphi_i dr \quad (24)$$

2.2.3 Loading arising from varied rotational speed

An additional loading is produced by a varied rotor speed, which is expressed as:

$$Q_{\Omega} = -\dot{\Omega} \int_0^L (\mu(r)r\phi_x(r))dr \quad (25)$$

Combining Eqs. (23)-(25) with Eq. (15), the equation of motion for an offshore wind turbine under forced vibration conditions can be obtained as:

$$M\ddot{q} + C\dot{q} + Kq = Q \quad (26)$$

where Q represents the sum of the generalized forces discussed above.

2.3 Aeroelastic effect

To account for the aeroelastic effect, the formula used in Section 2.2.1 must be modified because the structural velocity must be included in Eqs. (17) and (18). Then, the out-of-plane velocity V_y , in-plane velocity V_x , and relative velocity V_{rel} can be expressed as:

$$\begin{aligned} V_y &= \bar{V}(1-a) - \phi_y(r)\dot{q}_{yb,i} \\ V_x &= \Omega r(1+a') + \phi_x(r)\dot{q}_{xb,i} \end{aligned} \quad (27)$$

$$V_{i,rel}(r, t) = \sqrt{(\bar{V}(1-a) - \phi_y(r)\dot{q}_{yb,i})^2 + (\Omega r(1+a') + \phi_x(r)\dot{q}_{xb,i})^2} \quad (28)$$

2.4 Control system

A variable-speed, variable-pitch configuration is one typical control method, and relies on the design of two basic control systems: a generator-torque controller and a full-span rotor-collective blade-pitch controller. In the below-rated wind speed region, the generator-torque controller works to maintain the optimal tip-speed ratio. In the above-rated wind speed region, the blade-pitch controller works to ensure rated power-production.

Taking the control system of an NREL5MW baseline wind turbine as an example, the relationship between generator torque and generator speed is displayed in Fig. 7. A generator-torque controller works in region 2, where the optimal tip speed ratio is 7.55 and the generator efficiency is 94.4% [Jonkman, Butterfield, Musial et al. (2009)].

According to generator torque in Fig. 7, the rotor rotational acceleration $\Delta\dot{\Omega}$ can be obtained by:

$$T_{Aero} - N_{Gear}T_{Gen} = (I_{rotor} + N_{Gear}^2 I_{Gen}) \frac{d}{dt} (\Omega_0 + \Delta\Omega) = (I_{rotor} + N_{Gear}^2 I_{Gen}) \Delta\dot{\Omega} \quad (29)$$

where T_{Aero} is the rotor aerodynamic torque, T_{Gen} the generator torque, I_{rotor} the rotor moment of inertia, I_{Gen} the moment of inertia cast to the generator, Ω_0 the rated rotor rotational speed. Equations about dynamic loading in Section 2.2 and system matrices in Appendix A involving Ω should be replaced by $\Omega_0 + \Delta\Omega$, in which way the dynamic

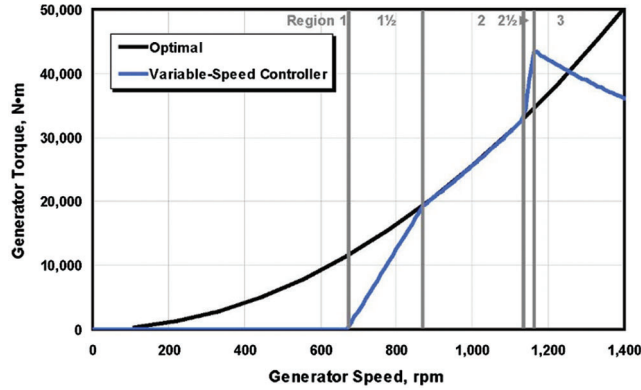


Figure 7: Relationship between generator torque and generator speed for NREL5MW baseline wind turbine [Jonkman, Butterfield, Musial et al. (2009)]

loading is determined by control system. For example, in-plane velocity V_x in Eq. (27) should be modified as:

$$V_x = (\Omega + \Delta\Omega)r(1 + a') + \phi_x(r)\dot{q}_{xb,i} \quad (30)$$

Moreover, a gain-scheduled proportional-integral (PI) control pattern is used for blade-pitch control in region 3, so the variation of the blade pitch angle $\Delta\beta$ can be expressed as:

$$\Delta\beta = K_P N_{Gear} \Delta\Omega + K_I \int_0^t N_{Gear} \Delta\Omega dt \quad (31)$$

where K_P and K_I represent the proportional gain and integral gain coefficient, respectively, and N_{Gear} is the high- to low-speed gearbox ratio. So that in Eqs. (7)-(8) and Eq. (20), blade pitch angle β should be substituted by $\beta + \Delta\beta$. In this way, not only the bi-axial elastic stiffnesses of the blade is changed, but also aerodynamic loading. For example, Eq. (20) is modified as:

$$o = \theta - \beta + \Delta\beta - \kappa \quad (32)$$

3 Numerical results

According to the above equations, the numerical model is established in Simulink software, and the parameters refer to the NREL 5 MW monopile foundation wind turbine [Jonkman and Musial (2010)]; several model properties are listed in Tab. 1.

Considering the pitch angle and the blade azimuth is 0, and the rotor is at a static state, the natural frequency calculated by the integrated model is compared with the result by FAST [Jonkman and Musial (2010)], as shown in Tab. 2:

The first two order frequencies calculated by FAST are slightly larger than the integrated model in this paper. This is because in the foundation module named SynDyn of the

Table 1: Properties of NREL 5 MW monopile wind turbine

Property index	Property description
Rated power	5 MW,
Cut-in, rated, cut-out wind speed	3, 11.4, and 25 m/s
Cut-in, rated rotor speed	6.9 and 12.1 rpm
Hub height	90 m
Rotor diameter	126 m
Blade mass	17,740 kg
Blade damping ratio	0.48%
Hub mass	56,780 kg
Nacelle mass	240,000 kg
Tower top diameter and thickness	3.87 m and 19 mm
Tower bottom diameter and thickness	6 m and 27 mm
Tower height	77.6 m
Tower damping ratio	1%
Pile penetration depth	36 m
Pile length	66 m
Pile diameter, thickness	6 m and 60 mm
Layered soil height (from bottom)	5, 9, and 22 m
Layered soil friction angle (from bottom)	33.0°, 35.0°, and 38.0°
Layered soil weight	10.0, 10.0, and 10.0 kg/m ²

Table 2: Frequency calculated by integrated model and FAST

Property index	Integrated model (Hz)	FAST (Hz)
1 st fore-aft bending mode	0.2518	0.254
1 st lateral bending mode	0.2525	0.254
1 st blade flapwise bending mode	0.715	0.707
1 st blade edgewise bending mode	1.0911	1.090

FAST program, a single pile is simulated as a beam fixed at both ends for finite element analysis. The comparison results show that the integrated model proposed in this paper is correct and can give sufficient accuracy. By eigenvalue analysis, the first eight orders of mode shapes and their corresponding natural frequency values are obtained for the integrated model, as shown in Fig. 8.

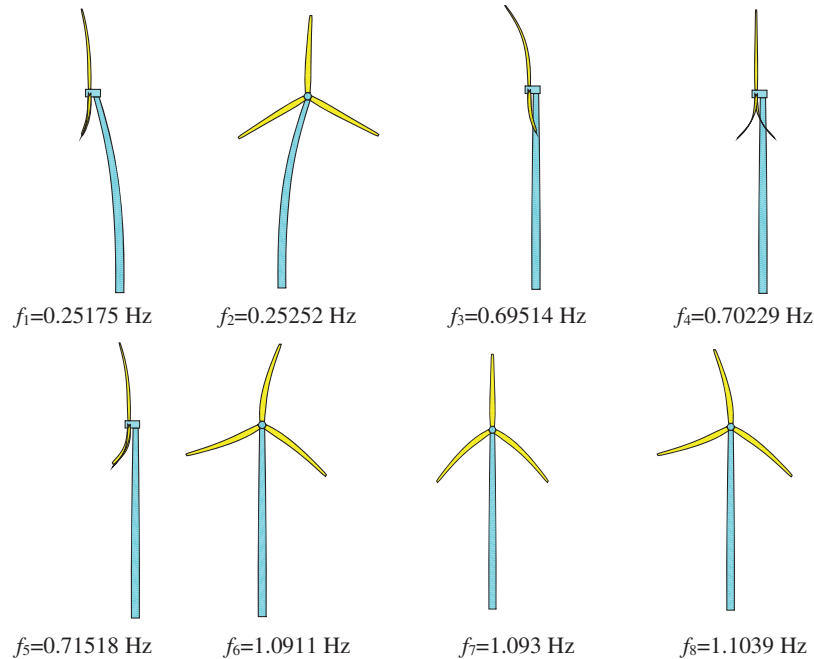


Figure 8: First eight orders of natural frequencies and mode shapes

Fig. 8 shows the plane in which the main deformation of the mode is generated. It can be seen from the figure that the first- and second-order modes are the overall fore-aft bending mode shape and lateral bending mode shape, and that there is a strong coupling effect between the supporting structure and blade. Frequency comparison between integrated model and topmass model is displayed in Tab. 3, and it can be found that the top mass model cannot reflect the frequency variety caused by the change in blade azimuth, pitch angle and rotation speed. Therefore, simplifying the rotor to the top mass of the tower is inaccurate in calculation. The higher-order modes from the third to the eighth order are mainly the local vibrations of the blade. The mode shape from the third to the fifth order is mainly characterized by the blade flapwise vibration. The mode shape from the sixth to the eighth order is mainly represented by the blade edgewise vibration, and the blade flapwise vibration and edgewise vibration are coupled.

4 Numerical results with scour depth varying

4.1 Frequency

In this paper, the 2.5-times pile diameter is taken as the maximum scour depth; that is, for a wind turbine with a pile diameter of 6 m, the maximum scour depth is 15 m. To obtain the influence of the scour depth on the frequency, this paper starts the calculation from without scouring, and the scour depth increases by 1 m at each step. For the purpose of understanding the influence of scour on the frequency of an offshore wind turbine with

Table 3: Frequency calculated by integrated model and top mass simplified model, where Scenario 1 represents blade 1 azimuth, pitch angle, and rotor speed are 0, and Scenario 2 represents blade 1 azimuth, rotor speed are 0, and pitch angle is $\pi/2$, and Scenario 3 represents pitch angle, rotor speed are 0, and pitch angle blade1 azimuth is $\pi/2$

Property index	Integrated model (Hz)			Top mass model (Hz)
	Scenario 1	Scenario 2	Scenario 3	
1 st fore-aft bending mode	0.2518	0.2522	0.2517	0.2524
1 st lateral bending mode	0.2525	0.2523	0.2525	0.2527
1 st blade flapwise bending mode	0.715	0.804	0.696	/
1 st blade edgewise bending mode	1.0911	1.2723	1.090	/

different soil parameters, the layered soil mentioned in the preceding section is replaced by uniform soil, and the lateral stiffness of the soil for a monopile foundation is represented by the horizontal resistance coefficient of foundation soil m . Four cases, $m=3 \times 10^6$, 4×10^6 , 5×10^6 , and 6×10^6 N/m⁴ are calculated, and the variation of the natural frequency of the wind turbine with scour depth is obtained as shown in Fig. 9.

The numerical results show that the first-, second-, fifth-, and eighth-order frequencies of the wind turbine change with the variation of the scour depth, and the relationship is shown in Figs. 9(a)-9(d), respectively, in which the unit of m is 10^6 N/m⁴. It can be seen from the above that the fifth- and eighth-order modes are high-order modes mainly based on blade vibration. Therefore, there is a coupling effect between the vibration of the support structure and that of the blade in the high-order mode. It can be seen from Fig. 9 that, for uniform soil, the natural frequency decreases linearly with increasing scour depth.

As for the case that $m=3 \times 10^6$ N/m⁴, from no scour to a scour depth of 15 m, the first- and second-order frequencies are reduced by 12.05%. Comparing the reduction rates of the first- and second-order frequencies with different horizontal resistance coefficients, they are 12.05%, 11.50%, 11.24%, and 11.18% with increasing m for first order and 12.05%, 11.59%, 11.26%, 11.15% for second order, it is found that the reduction rate of the natural vibration frequency with the scour depth decreases with increasing horizontal resistance coefficient of foundation soil.

Case 1 represents a state of the stationary wind turbine with a blade 1 azimuthal angle of 0° and a pitch angle of 0° . The blade parameters of the wind turbine are changed in case 2, in which the wind turbine with a rated rotational speed, a pitch angle of 90° and a blade 1 azimuthal angle of 90° . The scour depth is from 1 to 5 m, and the modal analysis is performed on the two cases separately, and the calculation results are shown in Fig. 10.

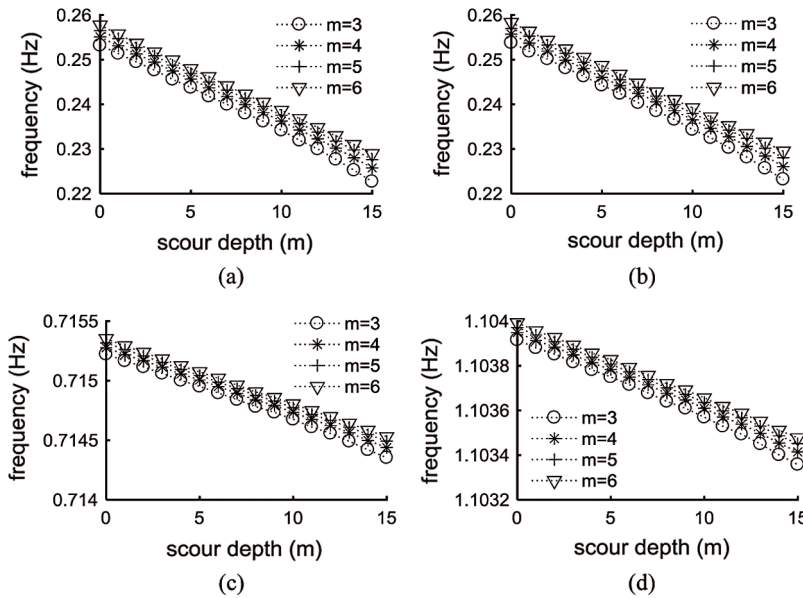


Figure 9: Multi-order natural frequency of offshore wind turbine vs. scour depth: (a) first-, (b) second-, (c) fifth-, and (d) eighth-order frequency

Results show that the first two modes of case 2 are exchanged with each other compared to the stationary wind turbine, due to the change of rotational speed, azimuthal angle, and pitch angle. This means that for case 2 the first-order mode is lateral vibration and the second-order mode is fore-aft vibration of the offshore wind turbine. For the high-order mode of case 2, although the blade vibration mode is the same, the overall vibration mode of the wind turbine is changed after coupling blade with the support structure. Specifically, the third to fifth mode shapes of case 2 are the sixth to eighth mode shapes in Fig. 9, and the sixth to eighth modes of case 2 are the third to fifth order mode shapes in Fig. 9. It can be seen from Fig. 10 that after considering the blade parameters the reduction rate of the first two modes of case 2 with scour depth is similar to that of case 1.

4.2 Mode shape

The mode shape of the wind turbine with a scour depth of 15 m is compared with that with no scouring, as shown in Fig. 11, from which it can be seen that the vibration mode of the first and second modes have changed after scouring.

To quantify the influence of the scour depth on the vibration modes, the bi-axial vibration mode factors of the three blade tips and the top of tower are taken to calculate the change with scour depth, which as shown in Fig. 12.

It is found from Fig. 12(a) that for the first-order mode, as scour depth increases, the tower-top fore-aft vibration mode factor increases continuously when the blade-tip flapwise vibration mode factor decreases. It can be seen from Fig. 12(c) that for the second-order

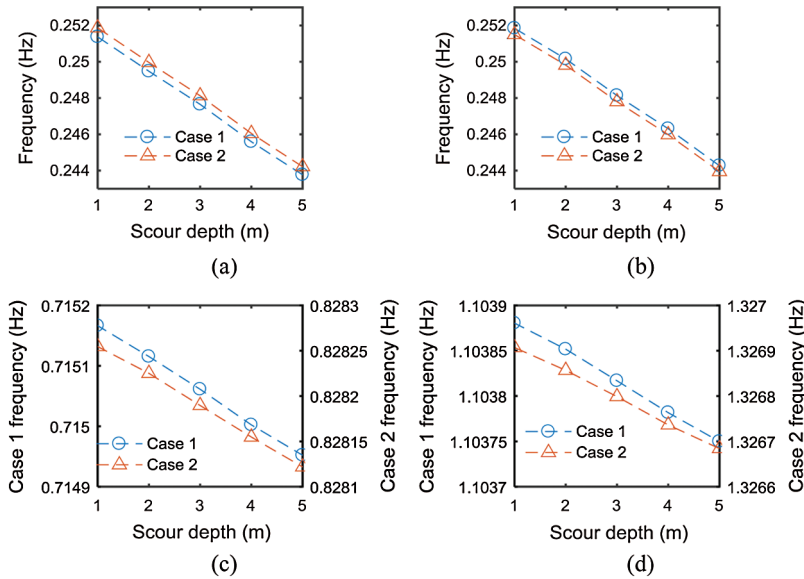


Figure 10: Multi-order natural frequency of offshore wind turbine vs. scour depth. Case 1, stationary wind turbine with blade 1 azimuthal angle of 0° and pitch angle of 0° ; case 2, wind turbine with rated rotational speed, pitch angle of 90° , and blade 1 azimuthal angle of 90° : (a) First-, (b) second-, (c) fifth-, and (d) eighth-order frequency

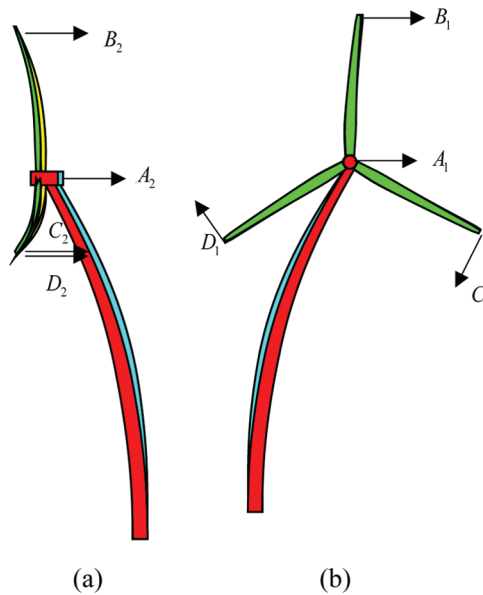


Figure 11: Mode-shape change of offshore wind turbine after scouring; cyan zone and yellow zone represent no scouring, and red zone and green zone represent the scour depth of 15 m. (a) First mode, fore-aft bending mode; (b) second mode, lateral bending mode

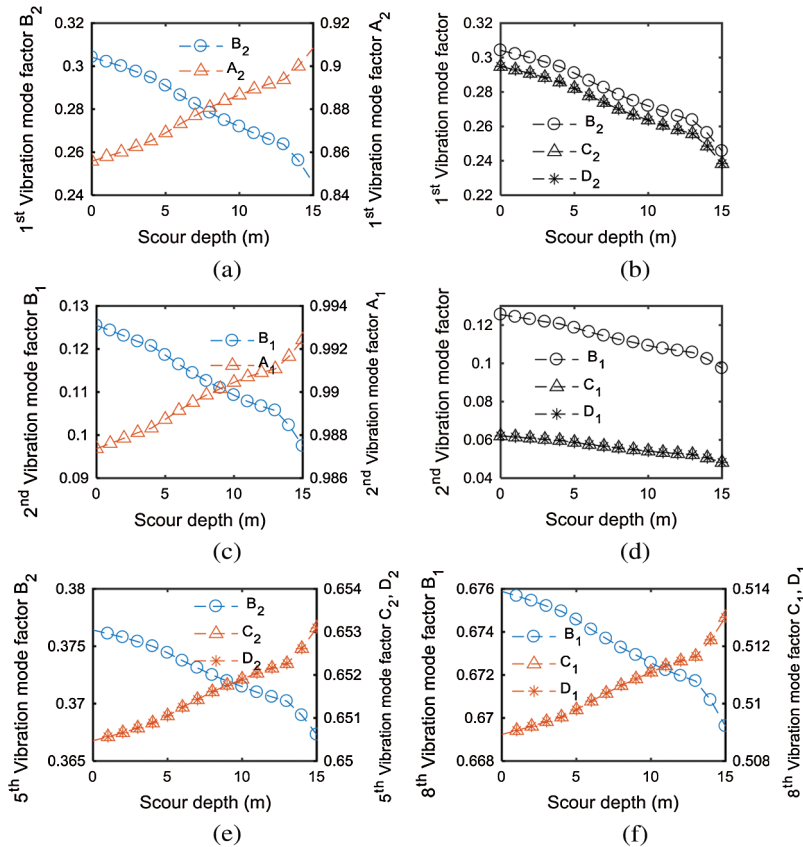


Figure 12: Vibration mode factor changes with scour depth; A_1 , A_2 , B_1 , B_2 , C_1 , C_2 , D_1 , and D_2 are shown in Fig. 11

mode the variation of the vibration mode factor of tower top and blade tip is the same as that of the first-order mode. It is found from Fig. 12(b) that for the first-order mode, although the three blade mode factors are reduced, the factor change of blades 2 and 3 (position is symmetric with respect to the tower center line) are the same, and different from that of blade 1 (position is vertically up). This indicates that the vibration mode factor change of the blade with scour depth is affected by the blade azimuth. Fig. 12(d) indicates the same. Figs. 12(e) and 12(f) show the variation of the blade flapwise vibration mode factor in the fifth-order mode and the blade edgewise vibration mode factor in the eighth-order mode, respectively. All of these figures show that the blade 1 vibration mode factor decreased with increasing scour depth, while the blades 2 and 3 vibration mode factors increased. These results illustrate that, for the global mode shape of an offshore wind turbine, scouring affects the vibration mode factors of the tower, monopile, and blades. The effect of the scour depth on the blade is related to the blade azimuth, and scouring has the same effect on the blades of the symmetrical position.

4.3 Displacement

The wind speed, soil parameters, and scour depth are used as variables to calculate the wind turbine time history response under uniform wind. Selecting wind speeds of 8, 12, and 15 m/s, scour depths from 0 to 15 m once every 1 m, and the soil parameters in Tab. 1 or uniform soil with $m=3 \times 10^6 \text{ N/m}^4$, a total of 96 conditions are obtained. The bi-axial tower-top displacements under different conditions are shown in Fig. 13.

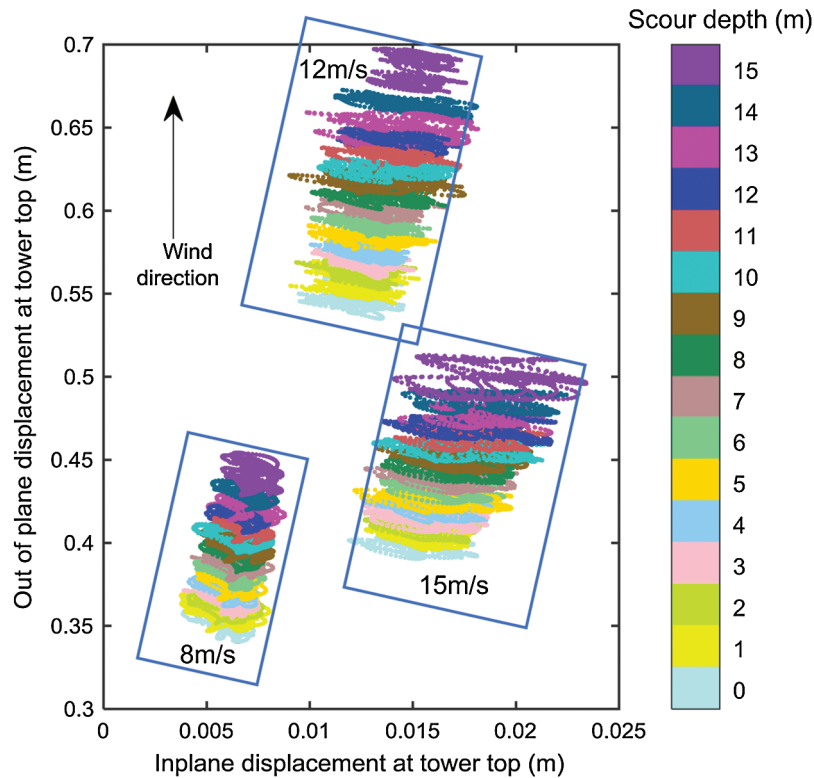


Figure 13: Distribution of tower-top position

The position of the tower top is calculated out by taking the in-plane and out-of-plane displacements of the tower top as the horizontal and vertical coordinates, respectively. It is seen from Fig. 13 that under uniform wind speed, the tower-top position is always in the first quadrant. At three different wind speeds, three non-coinciding concentrated areas are exhibited. Owing to the control system, when the wind speed exceeds the rated wind speed, the out-of-plane displacement of the tower is reduced. At the same wind speed, as the scour depth increases, the spatial distribution of the tower-top position moves away from the origin of the coordinate system. From Fig. 13, the scour depth can be estimated from the tower-top position at the known hub wind speed and known soil parameter

values. However, at the same wind speed, there is a coincident portion of the tower-top position at different scour depths, so the value of the scour depth must be further confirmed.

4.4 Rotation

The 96 conditions mentioned in Section 4.3 are used to calculate the time-history response of the pile bi-axial rotation at the mudline, and the results are plotted in Fig. 14.

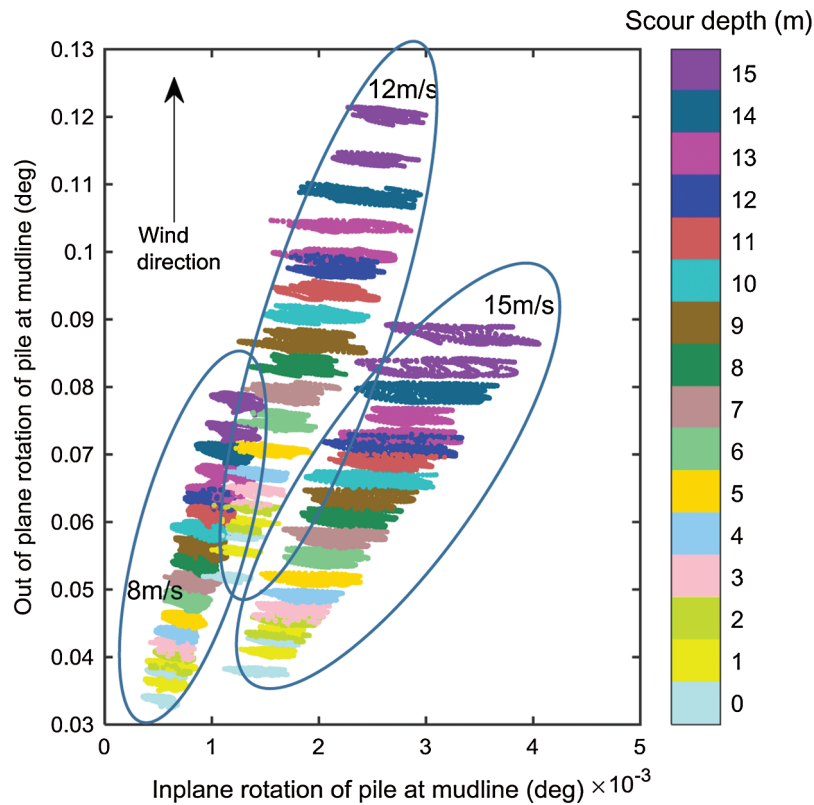


Figure 14: Distribution of pile rotation at mudline

The in-plane and out-of-plane pile rotations at the mudline are taken as the horizontal and vertical coordinates, and it can be seen from Fig. 14 that the rotation distribution at three wind speeds is also divided into three segments. Comparing Figs. 14 and 13, it can be found that the influence of the change of the scour depth on pile rotation at the mudline is more obvious than the tower-top displacement. At the same wind speed, the pile rotation distribution does not coincide under different scour depths. This means that under the specified wind speed and specified soil parameters, there is a specified pile rotation angle at the mudline corresponding to the specified scour depth. This provides an idea for the reverse problem of obtaining scour depth based on structural response.

Therefore, the scour depth can be obtained based on the known pile rotation angle at the mudline, while the wind speed and the soil parameter values are known.

5 Conclusions

Scouring causes a wind turbine foundation to be unstable, and monopile foundations, which are the mostly widely used, are more vulnerable than other foundations to scouring. Blades have always been simplified to mass in previous studies on the effects of scouring. In this paper, the coupling of the blade, tower, and monopile foundation is considered when calculating the influence of the scouring on the dynamic characteristics of the offshore wind turbine. On this basis, the aeroelastic effect and control system are also taken into consideration, and the influence of scouring on the wind-induced response of offshore wind turbines is calculated. The following conclusions can be drawn.

(1) The reduction rate of the natural vibration frequency with the scour depth decreases with increasing horizontal resistance coefficient of foundation soil. For a uniform soil, the natural frequency decreases linearly with increasing scour depth.

(2) The first two modes of a feathered and rated-rotational-speed wind turbine are exchanged with each other compared to a stationary offshore wind turbine. After considering the blade parameters, the reduction rate of the first two modes with the scour depth is similar to that of a stationary offshore wind turbine.

(3) For the global mode shape of an offshore wind turbine, scouring affects the vibration mode coefficients of the tower, monopile, and blades. The effect of scour depth on the blade is related to the blade azimuth, and scouring has the same effect on the blades of the symmetrical position.

(4) At the same wind speed, as the scour depth increases, the spatial distribution of the tower-top position moves away from the origin of the coordinate system. Therefore, the scour depth can be roughly estimated from the tower-top position at the known hub wind speed and known soil parameter values.

(5) The influence of the change of the scour depth on pile rotation at the mudline is more obvious than tower-top displacement. Therefore, the scour depth can be obtained based on known pile rotation angle at the mudline, while wind speed and the soil parameter values are known.

In a planned future study, one offshore wind turbine founded on a monopile on-site will be chosen as the research object, and the modeling method in this paper will be used to calculate the impact of scouring on its dynamic characteristics and wind-induced response.

Funding Statement: The author(s) received no specific funding for this study.

Conflicts of Interest: The authors declare that they have no conflicts of interest to report regarding the present study.

References

- Abhinav, K. A.; Saha, N.** (2016): Effect of scouring in sand on monopile-supported offshore wind turbines. *Marine Georesources & Geotechnology*, vol. 35, no. 6, pp. 817-828. DOI 10.1080/1064119X.2016.1255687.
- Davenport, A. G.** (1965): The relationship of wind structure to wind loading. *Proceedings of the Conference on Wind Effects on Buildings and Structures*. National Physical Laboratory, London, pp. 54-111.
- Fitzgerald, B.; Basu, B.** (2016): Structural control of wind turbines with soil structure interaction included. *Engineering Structures*, vol. 111, pp. 131-151. DOI 10.1016/j.engstruct.2015.12.019.
- Ho, A.; Mbistrova, A.; Corbetta, G.** (2016): *The European Offshore Wind Industry Key Trends and Statistics 2015*. Brussels, Belgium.
- Jonkman, J.; Butterfield, S.; Musial, W.; Scott, G.** (2009): *Definition of a 5-MW Reference Wind Turbine for Offshore System Development*. National Renewable Energy Laboratory (No. NREL/TP-500-38060), Golden, CO(United States).
- Jonkman, J.; Musial, W.** (2010): *Offshore Code Comparison Collaboration (OC3) for IEA Wind Task 23 Offshore Wind Technology and Deployment*. National Renewable Energy Laboratory, Golden, CO(United States).
- Lin, S. M.; Lee, S. Y.; Lin, Y. S.** (2008): Modeling and bending vibration of the blade of a horizontal-axis wind power turbine. *Computer Modeling in Engineering & Sciences*, vol. 23, no. 3, pp. 175-186.
- Pournazeri, S.; Li, S. S.; Haghghat, F. A.** (2015): A bridge pier scour model with non-uniform sediments. *Water Management*, vol. 167, no. 9, pp. 499-511.
- Prendergast, L. J.; Gavin, K.; Doherty, P.** (2015): An investigation into the effect of scour on the natural frequency of an offshore wind turbine. *Ocean Engineering*, vol. 101, pp. 1-11. DOI 10.1016/j.oceaneng.2015.04.017.
- Prendergast, L. J.; Reale, C.; Gavin, K.** (2018): Probabilistic examination of the change in eigenfrequencies of an offshore wind turbine under progressive scour incorporating soil spatial variability. *Marine Structures*, vol. 57, pp. 87-104. DOI 10.1016/j.marstruc.2017.09.009.
- Sørensen, S. P. H.; Ibsen, L. B.** (2013): Assessment of foundation design for offshore monopiles unprotected against scour. *Ocean Engineering*, vol. 63, pp. 17-25. DOI 10.1016/j.oceaneng.2013.01.016.
- Staino, A.; Basu, B.** (2013): Dynamics and control of vibrations in wind turbines with variable rotor speed. *Engineering Structures*, vol. 56, pp. 58-67. DOI 10.1016/j.engstruct.2013.03.014.
- Sumer, B. M.; Fredsøe, J.; Christiansen, N.** (1992): Scour around vertical pile in waves. *Journal of Waterway, Port, Coastal, and Ocean Engineering*, vol. 118, no. 1, pp. 15-31. DOI 10.1061/(ASCE)0733-950X(1992)118:1(15).

Van der Tempel, J.; Zaaier, M.; Subroto, H. (2004): The effects of scour on the design of offshore wind turbines. *Proceedings of 3rd International Conference on Marine Renewable Energy*. London, UK, pp. 27-35.

Veritas, D. N. (2010): *Offshore Standard DNV-OS-J101: Design of Offshore Wind Turbine Structures*. Det Norske Veritas, Høvik, Norway.

Yang, Z.; Peng, M.; Cao, Y.; Zhang, L. (2014): A new multi-objective reliability-based robust design optimization method. *Computer Modeling in Engineering & Sciences*, vol. 98, no. 4, pp. 409-442.

Zaaier, M. B. (2006): Foundation modelling to assess dynamic behaviour of offshore wind turbines. *Applied Ocean Research*, vol. 28, no. 1, pp. 45-57. DOI 10.1016/j.apor.2006.03.004.

Zaaier, M. B.; Van der Tempel, J. (2004): Scour protection, a necessity or a waste of money. *Proceedings of the 43 IEA Topical Expert Meeting*. Stockholm, pp. 43-51.

Zhang, Z. (2015): *Passive and Active Vibration Control of Renewable Energy Structures (Ph.D. Thesis)*. Aalborg University, Denmark.

Zhang, Z.; Li, J.; Nielsen, S. R. K.; Basu, B. (2014): Mitigation of edgewise vibrations in wind turbine blades by means of roller dampers. *Journal of Sound and Vibration*, vol. 333, no. 21, pp. 5283-5298. DOI 10.1016/j.jsv.2014.06.006.

Zhang, Z.; Nielsen, S.; Blaabjerg, F.; Zhou, D. (2014): Dynamics and control of lateral tower vibrations in offshore wind turbines by means of active generator torque. *Energies*, vol. 7, no. 11, pp. 7746-7772. DOI 10.3390/en7117746.

Appendix A. System matrices used in equations of motion

$$M = \begin{bmatrix} m_{2x} & 0 & 0 & 0 & 0 & 0 & a_1 & 0 \\ 0 & m_{2x} & 0 & 0 & 0 & 0 & a_2 & 0 \\ 0 & 0 & m_{2x} & 0 & 0 & 0 & a_3 & 0 \\ 0 & 0 & 0 & m_{2y} & 0 & 0 & 0 & b_1 \\ 0 & 0 & 0 & 0 & m_{2y} & 0 & 0 & b_2 \\ 0 & 0 & 0 & 0 & 0 & m_{2y} & 0 & b_3 \\ a_1 & a_2 & a_3 & 0 & 0 & 0 & N_m & 0 \\ 0 & 0 & 0 & b_1 & b_2 & b_3 & 0 & N_m \end{bmatrix} \quad (33)$$

where

$$N_m = 3m_0 + M_{hm}$$

$$a_i = m_{1x} \cos \varphi_i$$

$$b_i = m_{1y} \cos \varphi_i$$

$$m_0 = \int_0^L \mu(r) dr$$

$$m_{1x} = \int_0^L \mu(r) \phi_x(r) dr$$

$$m_{1y} = \int_0^L \mu(r) \phi_y(r) dr$$

$$m_{2x} = \int_0^L \mu(r) \phi_x^2(r) dr$$

$$m_{2y} = \int_0^L \mu(r) \phi_y^2(r) dr$$

$$K = \begin{bmatrix} k_{11} & 0 & 0 & k_{12} & 0 & 0 & 0 & 0 \\ 0 & k_{11} & 0 & 0 & k_{12} & 0 & 0 & 0 \\ 0 & 0 & k_{11} & 0 & 0 & k_{12} & 0 & 0 \\ k_{12} & 0 & 0 & k_{22} & 0 & 0 & 0 & 0 \\ 0 & k_{12} & 0 & 0 & k_{22} & 0 & 0 & 0 \\ 0 & 0 & k_{12} & 0 & 0 & k_{22} & 0 & 0 \\ e_1 & e_2 & e_3 & 0 & 0 & 0 & k_{31} & 0 \\ 0 & 0 & 0 & 0 & 0 & 0 & 0 & k_{32} \end{bmatrix} \quad (34)$$

where

$$k_{11} = k_{e,x} + k_{g,x} + k_{gr,x}$$

$$k_{22} = k_{e,y} + k_{g,y} + k_{gr,y}$$

$$k_{12} = k_c$$

$$e_i = -\Omega^2 \cos \varphi_i m_{1x}$$

$$k_{31} = k_{t,X} + k_{s,X} + k_{gr,X}$$

$$k_{32} = k_{t,Y} + k_{s,Y} + k_{gr,Y}$$

$$C = \begin{bmatrix} c_1 & 0 & 0 & 0 & 0 & 0 & 0 & 0 \\ 0 & c_2 & 0 & 0 & 0 & 0 & 0 & 0 \\ 0 & 0 & c_3 & 0 & 0 & 0 & 0 & 0 \\ 0 & 0 & 0 & c_4 & 0 & 0 & 0 & 0 \\ 0 & 0 & 0 & 0 & c_5 & 0 & 0 & 0 \\ 0 & 0 & 0 & 0 & 0 & c_6 & 0 & 0 \\ n_1 & n_2 & n_3 & 0 & 0 & 0 & c_7 & 0 \\ 0 & 0 & 0 & 0 & 0 & 0 & 0 & c_8 \end{bmatrix} \quad (35)$$

where

$$c_j = 2\zeta \sqrt{m_j k_j}$$

$$n_i = -2\Omega m_{1x} \sin \varphi_i$$